RSC Advances

PAPER

View Article Online
View Journal | View Issue

Cite this: *RSC Adv.*, 2020, **10**, 2180

Studies on the effects of different multiwalled carbon nanotube functionalization techniques on the properties of bio-based hybrid non-isocyanate polyurethane

Xin He, Xiaoling Xu, Guangxu Bo and Yunjun Yan *

A novel synthesis method for multiwalled carbon nanotube (MWCNT) modified bio-based hybrid non-isocyanate polyurethane (HNIPU) is proposed in this paper. Modification methods for several properties of MWCNTs–HNIPU were systematically studied. MWCNTs were grafted with carboxyl and amino groups using a condensation reflux device. Au nanoparticles were synthesized on the surface of the MWCNTs *via* a reduction reaction and Fe_3O_4 particles were decorated on the MWCNTs using a hydrothermal method. FTIR, TEM, XRD, XPS and Raman techniques were employed to confirm the compositions and structures. Then, five different types of MWCNT were utilized for blending with non-isocyanate polyurethane (NIPU) *via* solution methods. After curing with epoxy resin E-51, the cross-linked composites were applied as coatings. A series of tests demonstrated that HNIPU composited with MWCNTs–COOH–Au had the highest T_g value, the best thermal, thermodynamic and mechanical properties, and excellent pencil hardness, adhesion, flexibility and impact strength, while HNIPU composited with MWCNTs–COOH–NH_2 had the best water absorption and swelling properties. These results showed that the properties of hybrid non-isocyanate polyurethane can be adjusted *via* different MWCNT surface modification approaches or the addition of nanoparticles, so this kind of polyurethane has a vast development space for coating applications.

Received 23rd October 2019
Accepted 20th December 2019

DOI: 10.1039/c9ra08695a

rsc.li/rsc-advances

1. Introduction

As is well-known, polyurethanes have been widely applied in industry and daily life.[1,2] Among them, bio-based non-isocyanate polyurethanes (NIPUs) are a kind of green, sustainable and designable polyurethane,[3–6] as they use biomass as the substrate and they do not use isocyanate, a very highly toxic phosgene derivative, as a raw material, which provides them with an overwhelming advantage over traditional polyurethanes.[7,8] However, bio-based NIPUs still have some aspects that need to be improved for their industrial application. Conventionally, this type of NIPUs needs to react with certain appropriate resins, such as epoxy resin, amino resin, acrylic resin, silicone resin and ketone resin, to overcome their low molecular weights so as to obtain hybrid non-isocyanate polyurethanes (HNIPUs). HNIPU, a thermosetting composite with NIPU as the main structure and other resins as the crosslinking agent, possesses good properties.[9–11] Nevertheless, before the widespread use of HNIPUs, they still need application research and further improvement to meet industrial demand.

Multiwalled carbon nanotubes (MWCNTs) are composed of a number of concentric single walled nanotubes held together with relatively weak van der Waals forces.[12] Compared with common carbon materials, MWCNTs have exceptional thermal, mechanical, and electrical properties and high aspect ratios.[13,14] They have great potential as candidates for the reinforcement of polymer matrices. But, considering the uniform dispersion and compatibility between MWCNTs and matrices, developing long-term stable suspensions and proper applications in industry is becoming a research hotspot at present.[15,16] Zainuddin *et al.* dispersed functionalized MWCNTs–NH_2 in SC-15 epoxy with and without acetone medium by using a combination of an ultrasound processor and a 3-roll shear mixer, obtaining better interfacial bonding.[17] Guedes *et al.* prepared nanocomposites of ultra-high molecular weight polyethylene reinforced with MWCNTs, verifying that the MWCNTs did not change the viscoelastic nature of the ultra-high molecular weight polyethylene.[18] Kubĕna *et al.* obtained neat polyurethane specimens and composites of polyurethane with variable amounts of MWCNTs, finding that the addition of MWCNTs had less effect on the polymer matrix under low deformation than high

Key Laboratory of Molecular Biophysics of the Ministry of Education, College of Life Science and Technology, Huazhong University of Science and Technology, Wuhan 430074, China. E-mail: yanyunjun@hust.edu.cn; Fax: +86-27-87792213; Tel: +86-27-87792213

deformation.[19] Besides, new applications of composites with MWCNTs continuously come forth. Cao *et al.* developed several functional MWCNTs, and compared their absorption properties.[20] Luo *et al.* prepared a wear-resistant conductive superhydrophobic coating with a nest-like structure *via* a one-step method, which could be used in anti-electromagnetic interference, corrosion protection and anti-ice applications.[21] Though modified MWCNTs composited with polymers have been the focus of a few related reports in the literature, there is no report on HNIPUs composited with MWCNTs or functional MWCNTs, which are worth investigating and further exploring their new applications. Besides, the effect of functionalized MWCNTs on the properties of composites also needs to be carefully examined. In addition, the previous work of other researchers on MWCNT–polymer composites employed MWCNTs to enhance the thermal, mechanical and coating properties of the composites, but there lacks a comparison of the properties of differently modified MWCNT–polymer composites, especially MWCNTs that are loaded with nanoparticles.

Coatings, one of the most important applications of polyurethanes, need such properties as excellent hardness, flexibility, adhesive force, and impact and heat resistance. In contrast, single component epoxies or polyurethanes usually have corresponding disadvantages, such as less flexibility or poor heat resistance. Herein, the use of hybrid epoxy-hydroxyurethane compositions is proposed to overcome these bottlenecks.[2]

Therefore, in this work, five MWCNT bio-based hybrid non-isocyanate polyurethane composites and tinplate covered with coatings were investigated, and the MWCNT bio-based hybrid non-isocyanate polyurethane composites were firstly prepared and reported. The main study included: the synthesis of the five MWCNT powders, and then characterization to ascertain their structure; these powders were added into a NIPU solution for ultrasonic dispersion; finally, the mixtures were cured with epoxy resin, then formed into bulk specimens and covered on tin for characterization, respectively; after that, the effects of MWCNTs on the epoxy-hydroxyurethane composites were systematically examined *via* DSC, TGA, DMA, FSEM, XRD, AFM, water absorption, swelling and mechanical tests to explore their possibilities in coating applications by tailoring the groups on the MWCNTs.

2. Experimental

2.1 Materials

Multiwalled carbon nanotubes (purity: ≥97.0%; 3–15 nm in diameter and 15–30 nm in length; grade: technical grade; abbreviation: MWCNTs) were purchased from Shenzhen Tuling Evolution Technology Ltd Co. (Shenzhen, China). Gold chloride trihydrate (purity: ≥99.9%; grade: guaranteed reagent; $HAuCl_4 \cdot 3H_2O$) was bought from Shanghai Aladdin Bio-Chem Technology Ltd Co. (Shanghai, China). Non-isocyanate polyurethane (molecular weight: 6457 g mol^{-1}; prepared in the lab; abbreviation: NIPU) was obtained according to our previous work.[22] Bisphenol-A epoxy resin E-51 (purity: ≥99.0%; molecular weight: 392 g mol^{-1}; mean epoxy value: 0.51; grade: technical grade) was purchased from Yueyang Petrochemical Ltd Co. (Yueyang, China). Concentrated sulfuric acid (purity: ≥98.0%; grade: chemically pure; H_2SO_4), concentrated nitric acid (purity: 65.0–68.0%; grade: chemically pure; HNO_3), ethanediamine (purity: ≥99.0%; grade: analytical reagent; abbreviation: EDA), 1,3-dicyclohexylcarbodiimide (purity: ≥99.0%; grade: analytical reagent; abbreviation: DCC), trisodium citrate dehydrate (purity: ≥99.0%; grade: analytical reagent; $Na_3C_6H_5O_7 \cdot 2H_2O$), polyvinylpyrrolidone K-30 (molecular weight: 40 000 g mol^{-1}; grade: guaranteed reagent; abbreviation: PVP), ferric chloride hexahydrate (purity: ≥99.0%; grade: analytical reagent; $FeCl_3 \cdot 6H_2O$), ferrous sulfate heptahydrate (purity: ≥99.0%; grade: analytical reagent; $FeSO_4 \cdot 7H_2O$), sodium hydroxide (purity: ≥96.0%; grade: analytical reagent; NaOH), sodium dodecyl benzene sulfonate (purity: ≥88.0%; grade: analytical reagent; abbreviation: SDBS), methylene chloride (purity: ≥99.5%; grade: analytical reagent; CH_2Cl_2), ethyl alcohol (purity: ≥99.7%; grade: analytical reagent; CH_3CH_2OH), and dimethyl sulfoxide (purity: ≥99.0%; grade: analytical reagent; abbreviation: DMSO) were bought from Sinopharm Chemical Reagent Ltd Co. (Shanghai, China).

2.2 Synthesis of modified MWCNTs

2.2.1 MWNCTs. The purchased MWCNTs were not further purified and were directly added to NIPU for synthesis of the MWCNTs–HNIPU bulk specimens and coatings.

2.2.2 MWCNTs–COOH.[23] 5.00 g of MWCNTs and 100 mL of concentrated acid mixture were mixed ($V_{H_2SO_4} : V_{HNO_3} = 3 : 1$) in a 250 mL conical flask in an ultrasonic bath for 0.5 h. Then, the conical flask was kept in a 110 °C oil bath with magnetic stirring, connected to a condensation reflux device, and the system continued to react for 6 h. After cooling to room temperature, the mixtures were diluted with deionized water, filtered with 0.45 μm filter membrane, and washed until pH was near neutral. Subsequently, the wet powders were kept in an 80 °C drying oven for removing the water, and then ground with a mortar and pestle. Finally, the samples were sealed in a clear bottle for subsequent testing and use.

2.2.3 MWCNTs–NH_2.[24] 1.00 g of MWCNTs–COOH, 150.00 g of EDA and 20.00 g of DCC were rapidly added to a round-bottomed flask with a condensation reflux device. The mixtures were reacted at 120 °C in an oil bath with magnetic stirring for 48 h. After cooling to room temperature, the mixtures were diluted with ethyl alcohol, filtered with 0.45 μm filter membrane, and washed until pH was near neutral. Subsequently, the wet powders were kept in an 80 °C drying oven for removing the water, and then ground with a mortar and pestle. Finally, the samples were sealed in a clear bottle for subsequent testing and use.

2.2.4 MWCNTs–COOH–Au.[25] 0.050 g of MWCNTs–COOH and 42.25 mL of 20 mmol L^{-1} chloroauric acid were mixed in a round-bottomed flask and treated for 0.5 h in an ultrasonic bath. After the mixtures were diluted by 50.00 mL of deionized water, 4.250 g of PVP (as stabilizer) was added into the solution

and the system was heated to boiling with magnetic stirring. 2.00 mL of deionized water with 0.212 g of trisodium citrate dihydrate (as a reducing agent) was quickly added to the previous mixture, and kept boiling for 15 min. Subsequently, the heat source was turned off, and the mixture was stirred to room temperature. The mixture was filtered by 0.45 μm membrane, and washed with deionized water until pH was near neutral. The wet powders were kept at 80 °C in a drying oven for removing the water, and then ground with a mortar and pestle. Finally, the samples were sealed in a clear bottle for subsequent testing and use.

2.2.5 MWCNTs–COOH–Fe_3O_4.[26] 5.406 g of ferric chloride hexahydrate and 2.781 g of ferrous sulfate heptahydrate were dissolved in 250 mL of deionized water, and 0.400 g of MWCNTs–COOH was scattered among the previous mixture with ultrasonic treatment for 30 min. The system was kept under nitrogen and stirred with mechanical stirring in a 50 °C water bath for 30 min. Then, the system temperature was raised to 65 °C, and 6.0 mol L^{-1} NaOH solutions were dropwise added until pH was greater than 12 for 1 h. The system temperature was raised to 85 °C, and 0.250 g of SDBS was quickly added. The reaction mixture was kept stirring until it cooled to room temperature. Subsequently, the mixture was filtered with 0.45 μm filter membrane, and washed with deionized water until pH was near neutral. The mixture was loaded into a small beaker and frozen in a refrigerator overnight. Then, the frozen samples were dried in a freeze dryer for 24 h to remove the water. Finally, the solids were ground with a mortar and pestle, and sealed in a clear bottle for subsequent testing and use.

2.3 Preparation of pure HNIPU, MWCNTs–HNIPU and MWCNTs–HNIPU coatings

Firstly, 0.06 g of MWCNTs was added into a PE pipe that contained 5 mL of mixed solution (ethyl alcohol : dichloromethane = 1 : 1). Then, the mixture was treated by ultrasonic processing for 0.5 h at room temperature in an ultrasonic bath so that the MWCNTs could be uniformly distributed in the mixed solution. 3.00 g of non-isocyanate polyurethane and 20 mL of mixed solution (ethyl alcohol : dichloromethane = 1 : 1) were added into a 50 mL glass beaker, and dissolved fully with magnetic stirring. When the system turned clear, the MWCNT mixed solution was poured into the system and stirred with magnetic stirring for 1 h. 2.10 g of epoxy resin E-51 and the previous solution were mixed and stirred for 1 h. After ultrasonic treatment for 4 h, the mixtures were poured into a Teflon mold and casted onto tinplate, respectively, ready for different tests. Finally, the Teflon mold and tinplate were cured with a temperature programme in a vacuum drying oven: 60 °C for 12 h and then 90 °C for 4 h. This sample was named MWCNTs–HNIPU. Pure HNIPU was synthesized in the same manner as above, except that MWCNTs were not added. MWCNTs–COOH–HNIPU, MWCNTs–NH_2–HNIPU, MWCNTs–COOH–Au–HNIPU and MWCNTs–COOH–Fe_3O_4–HNIPU were synthesized in the same way. The only thing to note here is that mechanical stirring replaced magnetic stirring for MWCNTs–COOH–Fe_3O_4–HNIPU owing to the magnetic interference.

2.4 Fourier transform infrared (FTIR) spectroscopy

FTIR measurements were conducted on a Bruker Vertex 70 instrument with an attenuated total reflection (ATR) accessary. Powder samples and KBr were added into a quartz mortar, and ground using a quartz pestle. Then, they were pressured into a tablet for testing. The solid block MWCNTs–HNIPU samples were directly tested using the ATR accessary. Spectra were acquired over the range of 400–4000 cm^{-1} from 128 co-added scans at 4 cm^{-1} resolution at room temperature.

2.5 Transmission electron microscopy (TEM)

Morphological studies of the different MWCNTs were carried out by using a HT7700 HITACHI transmission electron microscope. Samples were added into ethyl alcohol and dispersed by ultrasonic treatment for 30 min. Then, the sample solution was dropped on a copper grid, and left to dry for testing.

2.6 X-ray diffraction (XRD)

The crystallization behaviors of the samples were studied by using an X'pert3 powder X-ray diffractometer. Different MWCNTs were filled into a glass groove, pressed with another piece of glass and placed on the instrument for recording the diffraction patterns with a 2θ range from 5° to 90° at 17° min^{-1}. The MWCNTs–HNIPU composites were cut to 10 mm × 10 mm flakelets and placed on the instrument for recording diffraction patterns with a 2θ range from 5° to 50° at 5° min^{-1}.

2.7 X-ray photoelectron spectroscopy (XPS)

The elemental compositions on the surface of the different MWCNTs were measured by using a Thermo Fisher ESCALAB 250Xi X-ray photoelectron spectrometer. The incident radiation was a monochromatic Al Kα X-ray.

2.8 Laser confocal Raman microspectroscopy

A Horiba Jobin Yvon LabRAM HR800 was used to analyze the structure of different MWCNTs at room temperature. The emission peak wavelength was 523 nm, and the test scope was from 100 to 4000 cm^{-1}.

2.9 Field emission scanning electron microscopy (FSEM)

The morphology of the MWCNTs–HNIPU composites was observed by using a sirion 200 FSEM instrument. All MWCNTs–HNIPU composites were freeze-fractured after a short immersing time in liquid nitrogen and sputter coated with a Au layer.

2.10 Thermogravimetric analysis (TGA)

To investigate the thermal stability of the MWCNTs–HNIPU composites, a PerkinElmer Pyris 1 TGA instrument was

employed and TGA was performed from room temperature to 600 °C with a heating rate of 10 °C min^{-1} in a N_2 atmosphere.

2.11 Differential scanning calorimetry (DSC)

A PerkinElmer Diamond DSC instrument was used to obtain the glass transition temperature (T_g) of the MWCNTs–HNIPU composites. The testing conditions were as follows: under a N_2 atmosphere, firstly, the temperature was increased to 150 °C at a rate of 30 °C min^{-1} and kept at 150 °C for 2 min; then, the temperature was decreased to −50 °C at a rate of 5 °C min^{-1} and kept at −50 °C for 2 min; finally, the temperature was increased to 150 °C at a rate of 10 °C min^{-1}. The last heating was recorded for analysis.

2.12 Dynamic mechanical analysis (DMA)

A PerkinElmer Diamond DMA instrument was employed to study the thermodynamic properties of the MWCNTs–HNIPU composites. The samples were cut into 1 mm × 10 mm × 30 mm rectangular blocks and kept for testing. The test conditions were set as follows: heating from −100 °C to 150 °C at a heating rate of 3 °C min^{-1} under a N_2 atmosphere with compaction mode.

2.13 Atomic force microscopy (AFM)

Surface morphology and the phase diagram of the MWCNTs–HNIPU composites were characterized by using an SPM9700 AFM instrument in tapping mode. All MWCNTs–HNIPU samples were cut into flat pieces for sticking on the sample stage. Then, the surface of the flat pieces was cleared with ethyl alcohol, dried at 60 °C for 24 h, and kept for testing.

2.14 Water absorption

To investigate the water resistance of all MWCNTs–HNIPU composites, the weight changes over time of a bulk specimen were precisely recorded before and after immersion in deionized water at room temperature. The specimens were taken out, immediately wiped with filter paper, and accurately weighed. The water absorption was calculated by the following equation:

$$\text{Water absorption } (\%) = \frac{W_t - W_0}{W_0} \times 100$$

where W_t and W_0 are the weight of samples after and before immersion in deionized water, respectively.

2.15 Swelling

Swelling testing was used as a characterized method of the crosslinking degree for all MWCNTs–HNIPU composites. DMSO was the immersion organic solvent. Firstly, a bulk specimen was immersed in DMSO. At set intervals, the specimen was taken out, wiped with filter paper, and accurately weighed. The swelling was calculated by the following equation:

$$\text{Swelling } (\%) = \frac{W_t - W_0}{W_0} \times 100$$

where W_t and W_0 are the weight of samples after and before immersion in DMSO, respectively.

2.16 Mechanical properties

The mechanical properties of all MWCNTs–HNIPU composites were measured by using a Hengsgrand WDW-2 universal testing machine using a dog-bone shape dumbbell specimen according to GB/T 18173.1-2012. After ten specimens were tested, the average value was calculated.

2.17 Coating properties

The thickness of the film was recorded using a TT150 Thickness Meter. After zero correction with the blank tin, each specimen was measured three times and the mean value was calculated. The adhesion property of the coatings was studied by using the cross cut test, as per the Chinese National Standard (GB/T 9286-1998). Pencil hardness of the coating was measured using a pencil hardness tester as per the Chinese National Standard (GB/T 6739-2006). Flexibility of the coating was tested by using a conical mandrel as per the Chinese National Standard (GB/T 1731-1993). Impact resistance of the coating was obtained using an impact tester as per the Chinese National Standard (GB/T 1732-1993).

3. Results and discussion

3.1 Characterization of the modified MWCNTs

FTIR spectra of the different MWCNTs are presented in Fig. 1. The unmodified MWCNTs have no apparent peaks except for a very weak one coming from the hydroxyl groups of residual moisture, while the modified MWCNTs have obvious peaks at 3400 cm^{-1} and 1633 cm^{-1}, which are ascribed to carboxyl groups (–OH and C=O). A closer look reveals that there is a weak peak at 1051 cm^{-1}, which is ascribed to the stretching vibration of C–N. MWCNTs–COOH–Au has the same characteristic peaks as MWCNTs–COOH, because Au has no obvious peak. An absorption peak

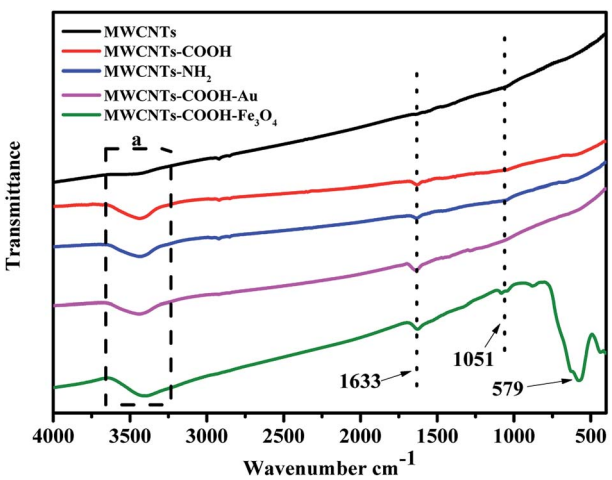

Fig. 1 FTIR spectra of different MWCNTs.

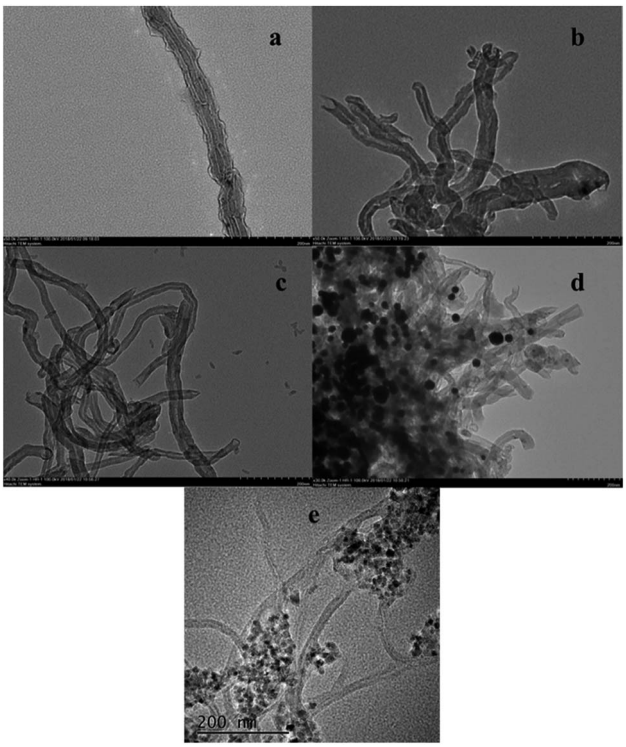

Fig. 2 TEM micrographs of different MWCNTs: (a) MWCNTs; (b) MWCNTs–COOH; (c) MWCNTs–NH_2; (d) MWCNTs–COOH–Au; (e) MWCNTs–COOH–Fe_3O_4.

at 579 cm^{-1} can be observed, which corresponds to the Fe–O vibration,[27] indicating that Fe_3O_4 nanoparticles existed on the MWCNTs. The existence of Au on the MWCNTs needs to be confirmed by other instruments.

Fig. 2 shows TEM images of the morphology of different MWCNTs. The surface of the unmodified MWCNTs is obviously not smooth according to Fig. 2a. In contrast, the surface of MWCNTs–COOH and MWCNTs–NH_2 is much smoother than that of the unmodified MWCNTs as they have been treated with strong acid. Furthermore, the ends of these two MWCNTs have already been opened, which illustrates that acid treatment can change the surface state of MWCNTs for a more convenient modification.[28] Meanwhile, many nanometer-sized Au and Fe_3O_4 particles can be observed on MWCNTs–COOH, of about 20–40 nm in size, showing that MWCNTs–COOH–Au and MWCNTs–Fe_3O_4 have been successfully synthesized.

Fig. 3 shows the XRD patterns of the different MWCNTs. For MWCNTs, MWCNTs–COOH and MWCNTs–NH_2, the strong diffraction peak at $2\theta = 26°$ can be indexed as the (0 0 2) reflection of the hexagonal graphite structure. The peak around 43° is due to the (1 0 0) graphitic planes.[29,30] After loading of Au nanoparticles, besides the diffraction peak of the MWCNTs, new peaks at 2θ values of 38° (1 1 1), 44° (2 0 0), 65° (2 2 0), 78° (3 1 1), and 82° (2 2 2) can be observed. And, for the Fe_3O_4 nanoparticles, new weak peaks at 2θ values of 30° (2 2 0), 35° (3 1 1), 43° (4 0 0), 57° (5 1 1), and 63° (4 4 0) can be observed, consistent with the standard XRD data for the cubic phase Fe_3O_4 (JCPDS no. 89-4319) with a face-centered cubic (fcc) structure.[31] However, the peak at a 2θ value of 26° (0 0 2) is hard to observe, because Fe_3O_4 wraps the MWCNTs. These results demonstrated the coexistence of Au and MWCNTs, and Fe_3O_4 and MWCNTs in the modified MWCNTs, separately.

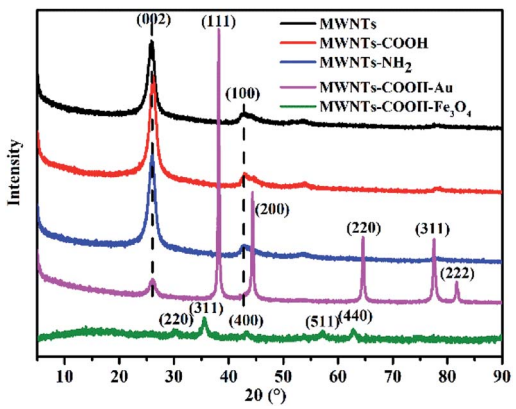

Fig. 3 XRD patterns of different MWCNTs.

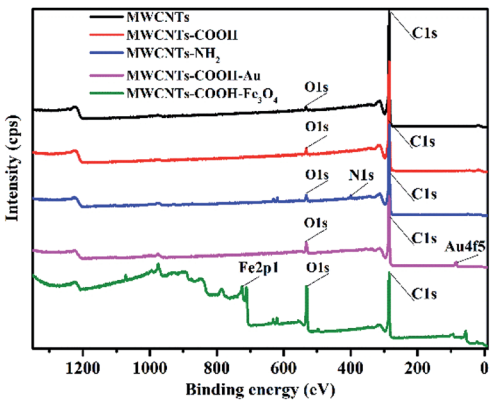

Fig. 4 XPS survey spectra of different MWCNTs.

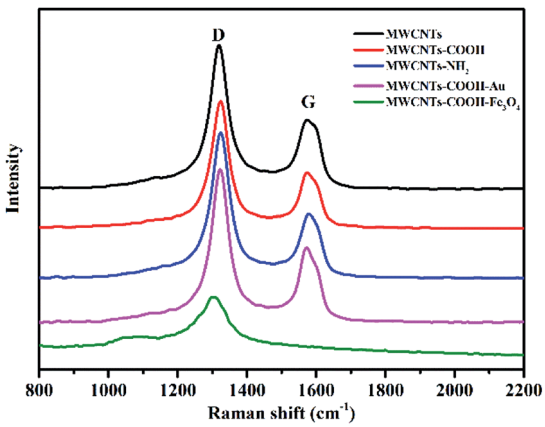

Fig. 5 Raman spectra of different MWCNTs.

Table 1 Raman data from different MWCNTs

	I_D/I_G
MWCNTs	1.8652
MWCNTs–COOH	2.2202
MWCNTs–COOH–NH_2	2.1757
MWCNTs–COOH–Au	2.0008
MWCNTs–COOH–Fe_3O_4	—

XPS analyses were employed to compare the chemical changes of different MWCNTs. Fig. 4 shows the XPS survey spectra recorded for the different MWCNTs. All MWCNTs have the same two peaks, the C 1s core level and the O 1s core level, which were at 284.8 eV and 531.9 eV, respectively. The unmodified MWCNTs have a weak peak at the O 1s core level, which can be attributed to adsorbed water molecules. After acid treatment, the peak at the O 1s core level exhibits an apparent rise for MWCNTs–COOH. The peak near 400.5 eV, observed for MWCNTs–NH_2, is generated by photoelectrons emitted from the N 1s core level. The binding energies of Au $4f_5$ and Fe $2p_1$ are located at 84.3 eV and 711.3 eV, respectively, indicating the formation of Au and Fe_3O_4 nanoparticles.[32,33] These results illustrated the successful synthesis of the modified MWCNTs.

Raman spectra were recorded to investigate the inner structural changes of different MWCNTs (Fig. 5). The peaks at 1348 and 1590 cm^{-1} corresponded to the D-band (the sp^3 defects of carbon atoms) and G-band (the sp^2 bonded carbon atoms), respectively.[34,35] The Raman I_D/I_G ratios (integral areas) are summarized in Table 1. After acid treatment, the value of the I_D/I_G ratio was obviously increased, confirming the presence of surface defects on the MWCNTs. Besides, the amino groups and Au nanoparticles can cover the surface defects of the MWCNTs according to the lower value of I_D/I_G than that of MWCNTs–COOH. Interestingly, MWCNTs–COOH–Fe_3O_4 has no G peak, which could be explained by the wrapping of Fe_3O_4, agreeing with the results from XRD testing.

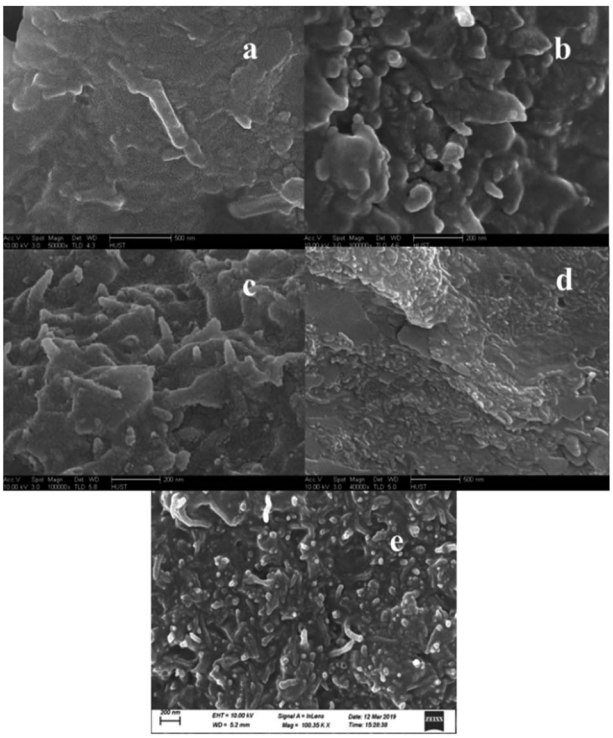

Fig. 7 FSEM micrographs of different MWCNTs–HNIPUs: (a) MWCNTs; (b) MWCNTs–COOH; (c) MWCNTs–NH_2; (d) MWCNTs–COOH–Au; (e) MWCNTs–COOH–Fe_3O_4.

3.2 Characterization of MWCNTs–HNIPUs and their coatings

Fig. 6 shows the FTIR spectra of different MWCNTs–HNIPU composites. They still show the characteristic functional groups of HNIPUs, like urethane groups at 1684 cm^{-1} and 1540 cm^{-1}, ester groups at 1649 cm^{-1} and methylene at 2942 cm^{-1} and 2836 cm^{-1}. These peaks indicate that the addition of different MWCNTs did not change the characteristic functional groups of HNIPUs except for

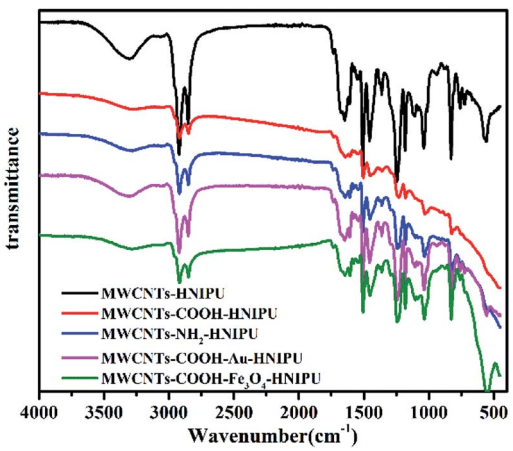

Fig. 6 FTIR spectra of different MWCNTs–HNIPUs.

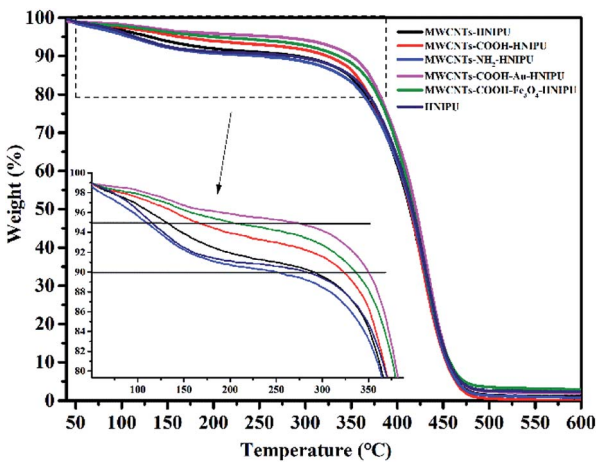

Fig. 8 TGA curves of different MWCNTs–HNIPUs and pure HNIPU.

the strong peak at 579 cm^{-1} from the Fe–O vibration of MWCNTs–COOH–Fe_3O_4–HNIPU.

The microstructural characteristics of the different MWCNTs–HNIPU composites were examined using FSEM and the results are displayed in Fig. 7. It clearly shows the dispersion of uniform MWCNTs, MWCNTs–COOH and MWCNTs–NH_2 within the matrix.[13,36] However, Au nanoparticles lead to some agglomeration of MWCNTs–COOH–Au in the composite, as is the case for the Fe_3O_4 nanoparticles. This phenomenon indicates that nanoparticles would greatly affect the dispersion of MWCNTs in HNIPU.

The results from TGA are shown in Fig. 8. With the addition of different MWCNTs, the decomposition temperatures at 5% weight loss of the composites are obviously increased compared to that of the pure HNIPU except for MWCNTs–NH_2–HNIPU. Especially, MWCNTs–COOH–Au–HNIPU has the best thermostability, reaching a decomposition temperature of 268.5 °C at 5% weight loss, which illustrates that Au nanoparticles can act as a heat sink for the composites. Fe_3O_4 nanoparticles have a similar effect on the composites, and can also improve the thermal stability of the composites, but the decomposition temperature at 5% weight loss only reached 200.3 °C. The weight loss can be used to estimate the functionalization efficiency.[37,38] The amino groups of the MWCNTs lead to the lowest decomposition temperatures at 5% weight loss, and a possible explanation is that MWCNTs–NH_2–HNIPU absorbs a lot of water, leading to more mass loss at low temperature. This result is consistent with the later result of water absorption.

The glass transition temperature (T_g) of different MWCNTs–HNIPU composites was obtained by using DSC (see Fig. 9). The midpoint temperature of the inflection between the onset and outset temperatures within the scope of the T_g range is set as T_g. The T_g of MWCNTs–COOH–Au–HNIPU has the highest value, reaching 22.62 °C; the T_g of MWCNTs–COOH–Fe_3O_4–HNIPU also has a high value of 18.41 °C, and this illustrates that nanoparticles on the MWCNTs can raise the T_g of composites. There is little difference between the values of the other MWCNTs–HNIPU composites and pure HNIPU, all being around 17 °C. Therefore, unmodified MWCNTs and modified MWCNTs could improve the glass transition temperature of the composites, except for MWCNTs–NH_2. Because the epoxy groups are added in the last step, the amino groups of MWCNTs–NH_2 would react with the epoxy groups to form a network structure, which is more conducive to molecular motion.[22]

The thermomechanical spectra of the different MWCNTs–HNIPU composites and pure HNIPU are presented in Fig. 10 (left) and (right). The results show that the addition of modified MWCNTs would increase the T_g (the temperature corresponding to the tan δ peak) of the composites, and MWCNTs–COOH–Au–HNIPU has the highest T_g, but the unmodified MWCNTs have no obvious effect on T_g. One explanation could be that dispersed MWCNTs and nanoparticles restrict the molecular motion,[39] leading to a higher T_g. Loss factor (tan δ) can also be used as a characterization

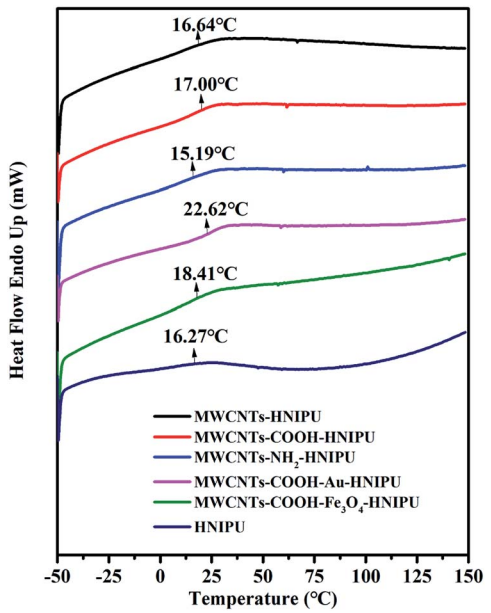

Fig. 9 The DSC curves of different MWCNTs–HNIPUs and pure HNIPU.

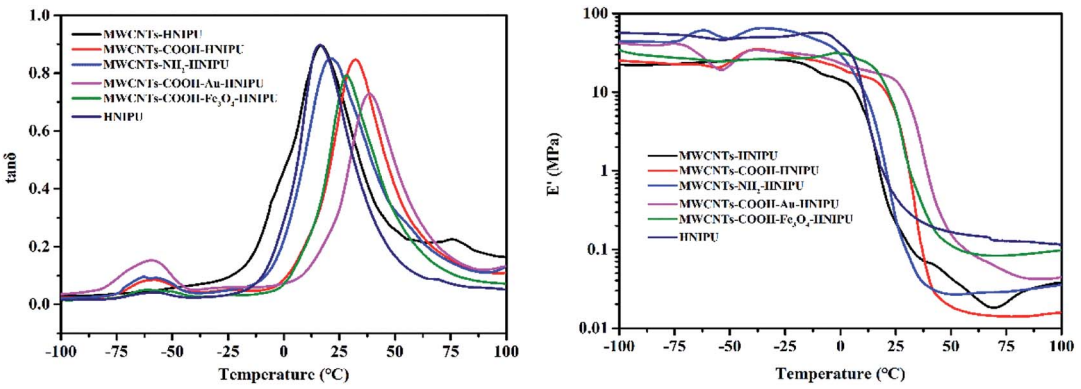

Fig. 10 The temperature dependence at 1 Hz of the tan δ (left) and storage modulus E' (right) values of different MWCNTs–HNIPUs and pure HNIPU.

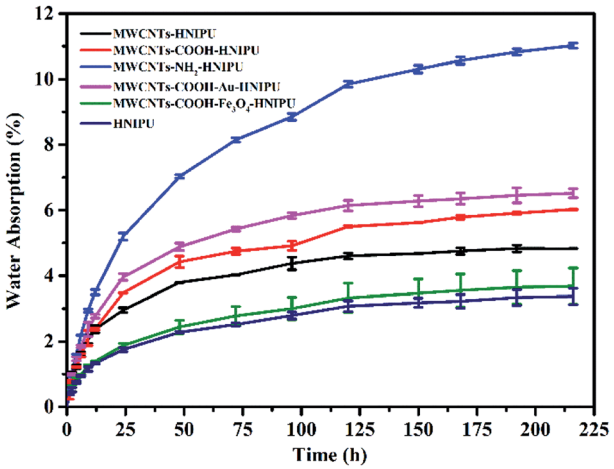

Fig. 11 The water absorption of different MWCNTs–HNIPUs and pure HNIPU.

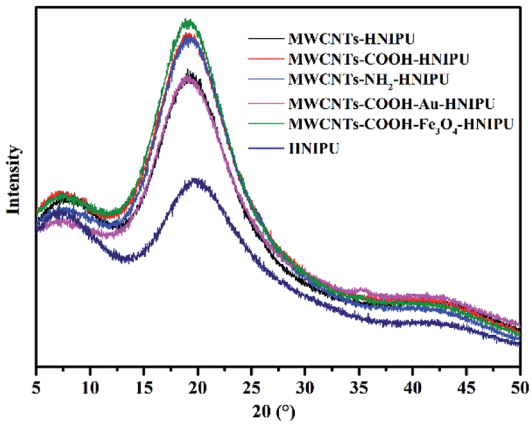

Fig. 13 X-ray diffraction patterns of different MWCNTs–HNIPUs and pure HNIPU.

parameter of damping properties.[40] A suitable range of temperature can enable more practical use at tan $\delta > 0.3$. With the addition of different MWCNTs, the range of temperature for tan $\delta > 0.3$ moves to a high temperature range, and all of them cover room temperature (25 °C). These results suggested that MWCNTs can enhance the damping properties to move the temperature range higher, especially for MWCNTs–COOH–Au–HNIPU. It can be noted that modified MWCNTs give a higher E' than pure HNIPU and unmodified MWCNTs–HNIPU at room temperature, especially carboxyl modified MWCNTs. These observations indicate that the content of different MWCNTs is responsible for the stiffness and viscoelastic properties of the composites,[41] which is consistent with the DSC results.

Fig. 11 shows the water absorption of different MWCNTs–HNIPU composites and pure HNIPU. Obviously, the addition of different MWCNTs can increase the water absorption ability of the composites. The main reason could be ascribed to conduits, which are made of these MWCNTs. Besides, MWCNTs–NH_2 have a hydrophilic group (–NH_2), contributing to the higher water absorption than other MWCNTs. In particular, water absorption of the composites is greatly affected by the hydrophilicity of these MWCNTs. According to the experimental results, the water absorption of HNIPU is very low, only about 2%. In comparison, the unmodified

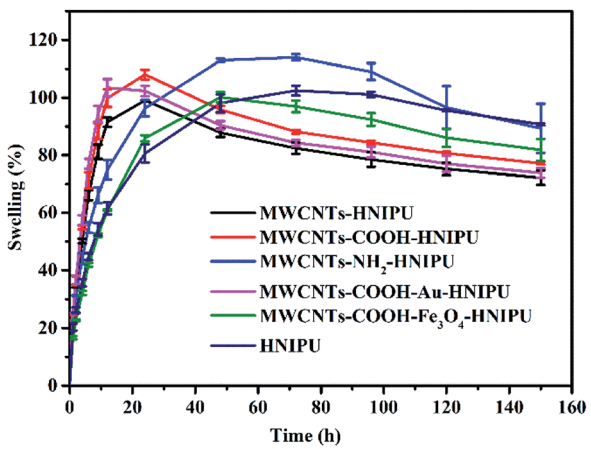

Fig. 12 The swelling of different MWCNTs–HNIPUs and pure HNIPU.

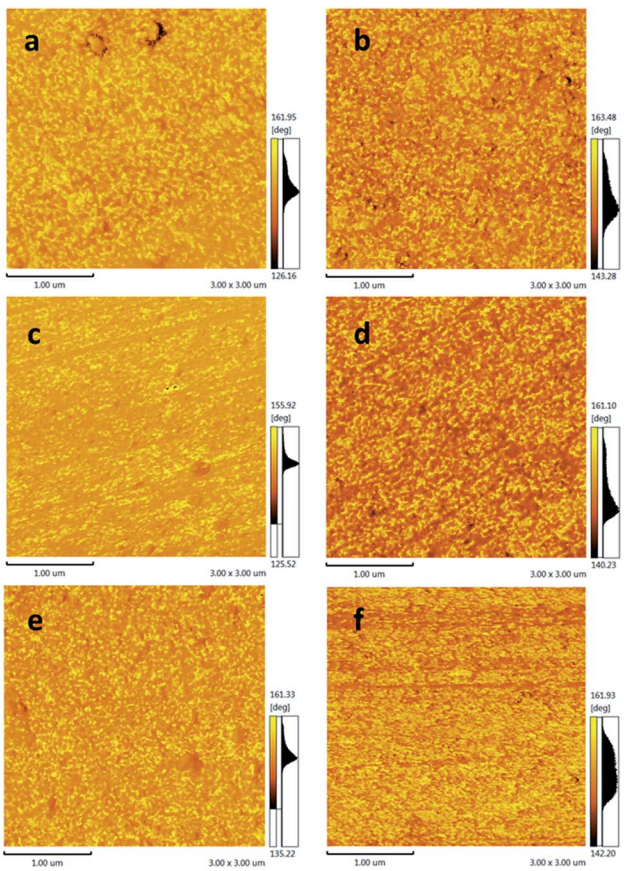

Fig. 14 The two-dimensional AFM phase diagrams of different MWCNTs–HNIPUs and pure HNIPU: (a) MWCNTs–HNIPU; (b) MWCNTs–COOH–HNIPU; (c) MWCNTs–NH_2–HNIPU; (d) MWCNTs–COOH–Au–HNIPU; (e) MWCNTs–COOH–Fe_3O_4–HNIPU; (f) pure HNIPU.

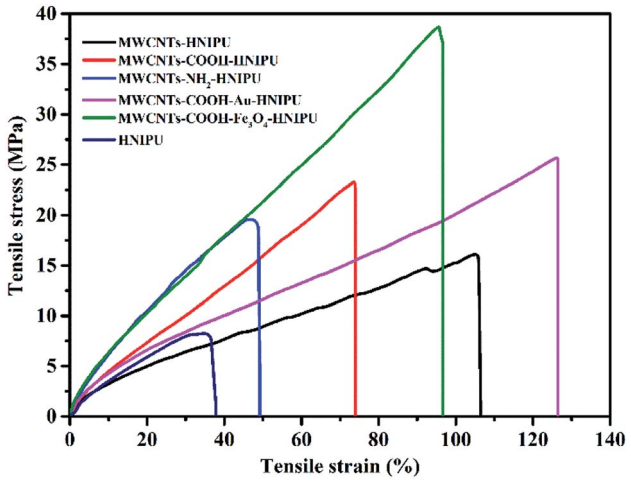

Fig. 15 The strain–stress curves of different MWCNTs–HNIPUs and pure HNIPU.

MWCNTs could produce gaps to let water in. The hydrophobicity of Fe_3O_4 makes the composites less able to absorb water than the unmodified MWCNTs, and the hydrophilicity of the nano Au boosts water absorption. So, water absorption of HNIPU can be designed by switching the surface wettability of the MWCNTs.

Swelling represents the crosslinking degree of the composites and it can be studied using DMSO absorption at room temperature over time. In the first 20 h, with the addition of different MWCNTs, the swelling of the composites was higher than that of the pure HNIPU, which could be explained since the MWCNTs acted as conduits, making it easier for DMSO to enter the molecular gaps. After 20 h, the swelling of the composites decreased to different degrees, but not for MWCNTs–NH_2–HNIPU. As MWCNTs–NH_2 have reactive groups (amino groups), the composites can crosslink epoxy resin with the amino groups, leading to the highest swelling ability, meaning a higher crosslinking degree than that of the others. Another reason is that the amino groups of MWCNTs–NH_2 are hydrophilic, so they can absorb the more polar solvent of DMSO (Fig. 12).

Fig. 13 shows the X-ray diffraction patterns for the different MWCNTs–HNIPU composites and pure HNIPU. The diffractograms exhibit broad peaks at 2θ angles around 8, 19, and 43°, which are assigned to the scattering from HNIPU chains with regular interplanar spacing, indicating some degree of crystallinity.[42] There is no peak at 11° 2θ, illustrating that all composites are soft NIPU.[43] In comparison with pure HNIPU, the peak at 19° 2θ is increased for the composites, which is ascribed to the crystallization of these MWCNTs.

The two-dimensional AFM images of all composites are presented in Fig. 14. The dark color region of the images represents the hard segment and the bright color region represents the soft segment.[44] Comparing with the pure HNIPU, the hard segments are increased with the addition of different MWCNTs, indicating that all MWCNTs can increase the proportion of hard segments. According to Fig. 14a–e, all composites are apparently heterogeneous, showing that different MWCNTs have no significant effect on microphase separation. Among them, MWCNTs–NH_2 assemble hard segments together, which can be explained by the fact that the highly reactive groups (amino groups) can react with epoxy resin and hinder the microphase separation of the composites.

Fig. 15 shows the stress–strain curves of different MWCNTs–HNIPUs and pure HNIPU, and Table 2 shows the data on mechanical properties, aiming to study the effect of MWCNT modification on the mechanical properties. Compared to pure HNIPU, the addition of MWCNTs can significantly improve the breaking stress and elongation at break, especially for MWCNTs–COOH–Au–HNIPU and MWCNTs–COOH–Fe_3O_4–HNIPU. The young's modulus, tensile stress, and elongation at break of these two composites are 42.24 MPa, 26.65 MPa and 126.11%, and 61.96 MPa, 38.68 MPa and 95.62%, respectively, demonstrating that the nanoparticles could provide even more dramatic improvements than the others. In the meantime, according to the results from swelling, tensile strain is increased as crosslinking degree is decreased, suggesting that MWCNTs can be used as a bridge to connect composites so that the tensile strain and tensile stress are improved.

The coating properties of different MWCNTs–HNIPU composites and pure HNIPU are listed in Table 2. The pure HNIPU has the lowest thickness of all composites, because MWCNTs could attach and contain more mixed solution on the surface of tin, leading a thicker coating layer. Unmodified MWCNTs have little effect on the pencil hardness of the composites, it being the same as the pencil hardness of the pure HNIPU. Other modified MWCNTs could enhance the pencil hardness of the composites because of

Table 2 The mechanical properties of different MWCNTs–HNIPUs and pure HNIPU

Sample	Young's modulus (MPa)	Breaking stress (MPa)	Elongation at break (%)	Thickness (μm)	Pencil hardness	Flexibility	Adhesion	Impact resistance (cm)
MWCNTs–HNIPU	32.13 ± 3.07	16.08 ± 1.93	105.13 ± 3.77	873.3 ± 15.2	B	7	0	50
MWCNTs–COOH–HNIPU	44.12 ± 2.34	23.29 ± 1.69	73.62 ± 2.54	878.3 ± 13.7	HB	7	0	50
MWCNTs–NH_2–HNIPU	62.72 ± 2.59	19.57 ± 1.22	46.18 ± 2.47	863.3 ± 16.3	HB	7	0	50
MWCNTs–COOH–Au–HNIPU	42.24 ± 4.33	25.65 ± 2.55	126.11 ± 4.63	908.3 ± 12.9	HB	7	0	50
MWCNTs–COOH–Fe_3O_4–HNIPU	61.96 ± 3.68	38.68 ± 1.74	95.62 ± 3.53	816.7 ± 26.2	HB	7	0	50
Pure HNIPU	34.35 ± 1.83	8.24 ± 0.64	35.07 ± 1.46	169.0 ± 12.5	B	7	0	50

the reaction between functional groups. Other coating properties are as good as those of the pure HNIPU, illustrating that they would be not affected by different MWCNTs. In the meantime, these results indicate that these composites have potential application in adhesives and coatings.

4. Conclusions

In summary, five MWCNT powders were synthesized successfully and then utilized in composites with HNIPU for coating applications. It was observed that the modified MWCNTs had more of an effect than the unmodified MWCNTs, especially on the glass transition temperature, thermostability, and thermodynamic and mechanical properties. HNIPU composited with MWCNTs–COOH–Au had the best 5% weight loss, reaching 268.5 °C, and the highest T_g value obtained from DSC and DMA. The storage modulus of MWCNTs–COOH–Au–HNIPU was also the highest of all the composites at room temperature. With the addition of MWCNTs, the water absorption of the composites increased, and MWCNTs–NH_2–HNIPU exhibited the highest value because of the presence of hydrophilic groups. Meanwhile, due to the activity of the amino groups, the crosslinking degree of MWCNTs–NH_2–HNIPU was obviously higher than that of the other composites, according to the swelling results. These MWCNTs can enhance the thermal and mechanical properties, and the pencil hardness of coatings, especially the modified MWCNTs. In all, carboxy groups, Au nanoparticles and Fe_3O_4 nanoparticles on MWCNTs can enhance the thermal and mechanical properties, while amino groups on MWCNTs can improve the water absorption and swelling. In view of their thermostability, alterable water absorption, pencil hardness, flexibility, adhesion and impact resistance, these composites can be used as lower water absorption and heat resistant coatings.

Conflicts of interest

The authors declare no conflicts of interest.

Acknowledgements

This study was financially supported by the Project of Postdoctoral Science and Technology Activities in Hubei Province (0106170092), the National Natural Science Foundation of China (No. 31070089, 31170078 and J1103514), the National High Technology Research and Development Program of China (No. 2011AA02A204, 2013AA065805), the National Natural Science Foundation of Hubei Province (grant No. 2015CFA085) and the Fundamental Research Funds for HUST (No. 2014NY007, 2017KFXKJC010, 2017KFTSZZ001). The authors would like to acknowledge the Analytical and Testing Center of HUST for their valuable assistance with FTIR, TEM, FSEM, DSC, TGA and DMA measurements.

References

1 M. S. Kathalewar, P. B. Joshi, A. S. Sabnis and V. C. Malshe, *RSC Adv.*, 2013, **3**, 4110.
2 G. Rokicki, P. G. Parzuchowski and M. Mazurek, *Polym. Adv. Technol.*, 2015, **26**, 707.
3 O. L. Figovsky, L. Shapovalov and O. Axenov, *Surf. Coat. Int., Part B*, 2004, **87**, 83.
4 O. Türünç, N. Kayaman-Apohan, M. V. Kahraman, Y. Menceloğlu and A. Güngör, *J. Sol-Gel Sci. Technol.*, 2008, **47**, 290.
5 A. Cornille, R. Auvergne, O. Figovsky, B. Boutevin and S. Caillol, *Eur. Polym. J.*, 2017, **87**, 535.
6 H. Blattmann, M. Fleischer, M. Bähr and R. Mülhaupt, *Macromol. Rapid Commun.*, 2014, **35**, 1238.
7 H. Asemani, F. Zareanshahraki and V. Mannari, *J. Appl. Polym. Sci.*, 2019, **136**, 47266.
8 J. Ke, X. Li, S. Jiang, C. Liang, J. Wang, M. Kang, Q. Li and Y. Zhao, *Polym. Int.*, 2018, **68**, 651.
9 K. Wazarkar, M. Kathalewar and A. Sabnis, *Eur. Polym. J.*, 2016, **84**, 812.
10 S. Doley, A. Sarmah, C. Sarkar and S. K. Dolui, *Polym. Int.*, 2018, **67**, 1062.
11 J. Ke, X. Li, F. Wang, M. Kang, Y. Feng, Y. Zhao and J. Wang, *J. CO2 Util.*, 2016, **16**, 474.
12 E. T. Thostenson, Z. Ren and T. Chou, *Compos. Sci. Technol.*, 2001, **61**, 1899.
13 X. Xu, Z. Li, L. Shi, X. Bian and Z. Xiang, *Small*, 2007, **3**, 408.
14 Y. V. Yakovlev, Z. O. Gagolkina, E. V. Lobko, I. Khalakhan and V. V. Klepko, *Compos. Sci. Technol.*, 2017, **144**, 208.
15 M. R. Loos, J. Yang, D. L. Feke, I. Manas-Zloczower, S. Unal and U. Younes, *Composites, Part B*, 2013, **44**, 740.
16 S. Hsu, C. Chou and S. Tseng, *Macromol. Mater. Eng.*, 2004, **289**, 1096.
17 S. Zainuddin, A. Fahim, T. Arifin, M. V. Hosur, M. M. Rahman, J. D. Tyson and S. Jeelani, *Compos. Struct.*, 2014, **110**, 39.
18 R. M. Guedes, C. M. C. Pereira, A. Fonseca and M. S. A. Oliveira, *Compos. Struct.*, 2013, **105**, 263.
19 M. Kuběna, M. Eliáš, L. Zajíčková, J. Poduška and T. Kruml, *Adv. Mater. Sci. Eng.*, 2019, **2019**, 1.
20 M. Cao, J. Yang, W. Song, D. Zhang, B. Wen, H. Jin, Z. Hou and J. Yuan, *ACS Appl. Mater. Interfaces*, 2012, **4**, 6949.
21 X. Luo, M. Wei, M. Cao, H. Ren and J. Feng, *Chem. Eng. Process.*, 2018, **131**, 27.
22 X. He, X. Xu, Q. Wan, G. Bo and Y. Yan, *Polymers*, 2019, **11**, 1026.
23 J. Xiong, D. Zhou, Z. Zheng, X. Yang and X. Wang, *Polymer*, 2006, **47**, 1763.
24 T. Ramanathan, F. T. Fisher, R. S. Ruoff and L. C. Brinson, *Chem. Mater.*, 2005, **17**, 1290.
25 K. R. Reddy, B. C. Sin, K. S. Ryu, J. Kim, H. Chung and Y. Lee, *Synth. Met.*, 2009, **159**, 595.
26 L. Kong, X. Lu and W. Zhang, *J. Solid State Chem.*, 2008, **181**, 628.
27 J. Wang, S. Zheng, Y. Shao, J. Liu, Z. Xu and D. Zhu, *J. Colloid Interface Sci.*, 2010, **349**, 293.
28 G. Wu, Y. Fan, X. He and Y. Yan, *RSC Adv.*, 2015, **5**, 8889.
29 P. Saini, V. Choudhary, B. P. Singh, R. B. Mathur and S. K. Dhawan, *Mater. Chem. Phys.*, 2009, **113**, 919.

30 L. Ai, C. Zhang, F. Liao, Y. Wang, M. Li, L. Meng and J. Jiang, *J. Hazard. Mater.*, 2011, **198**, 282.
31 K. B. Narayanan and N. Sakthivel, *J. Hazard. Mater.*, 2011, **189**, 519.
32 G. Wei, C. Pan, J. Reichert and K. D. Jandt, *Carbon*, 2010, **48**, 645.
33 A. Felten, C. Bittencourt and J. J. Pireaux, *Nanotechnology*, 2006, **17**, 1954.
34 S. Ye, X. Zhou, Y. Xu, W. Lai, K. Yan, L. Huang, J. Ling and L. Zheng, *Chem. Eng. J.*, 2019, **373**, 880.
35 T. McNally, P. Pötschke, P. Halley, M. Murphy, D. Martin, S. E. J. Bell, G. P. Brennan, D. Bein, P. Lemoine and J. P. Quinn, *Polymer*, 2005, **46**, 8222.
36 M. Raja, S. H. Ryu and A. M. Shanmugharaj, *Eur. Polym. J.*, 2013, **49**, 3492.
37 A. Tanver, M. Huang and Y. Luo, *RSC Adv.*, 2016, **6**, 49101.
38 S. Li, X. Du, C. Hou, X. Hao, J. Jia, T. Guan, T. Yi and G. Ma, *Compos. Sci. Technol.*, 2017, **143**, 46.
39 H. Xia and M. Song, *Soft Matter*, 2005, **1**, 386.
40 C. Zhang, Y. Chen, H. Li and H. Liu, *RSC Adv.*, 2018, **8**, 27390.
41 S. Gaidukovs, V. Kampars, J. Bitenieks, I. Bochkov, G. Gaidukova and U. Cabulis, *Integr. Ferroelectr.*, 2016, **173**, 1.
42 F. Wei, S. Enhai, F. Akihiko, W. Hongcai, N. Koichi and Y. Katsumi, *Bull. Chem. Soc. Jpn.*, 2000, **73**, 2627.
43 G. Trovati, E. A. Sanches, S. C. Neto, Y. P. Mascarenhas and G. O. Chierice, *J. Appl. Polym. Sci.*, 2010, **115**, 263.
44 D. Xiang, M. Liu, G. Chen, T. Zhang, L. Liu and Y. Liang, *RSC Adv.*, 2017, **7**, 55610.

